Progress In Electromagnetics Research C, Vol. 84, 35–46, 2018

Research on the Key Issues in Power and Data Wireless Transmission of Implantable Medical Devices

Xueping Li, Yuan Yang*, and Ningmei Yu

Abstract—In order to solve a key issue about power and data wireless transmission of implantable medical devices, M-ary differentially-encoded amplitude and phase-shift Keying (MDAPSK) is employed to balance the frequency selective contradiction in this paper. Subsequently, bio-capacitor model and biological path loss model are introduced to improve the accuracy of conventional wireless power transmission efficiency model. Based on 16DAPSK modulation, biological channel error rate analysis model is set up. Compared with experiment data, accuracy of the model is proved. Error codes suppression and error codes correction methods are optimized, and the optimization results have been verified by experiments. Lastly, it can be found that the power and data synchronized wireless transmission scheme is feasible. This work provides a new solution and model reference for power and data wireless transmission of implantable medical devices.

1. INTRODUCTION

The research of implantable medical devices, such as visual prosthesis, endoscopic capsule and nerve stimulators, belong to the interdisciplinary subject of biomedical and electronic information. As a powerful auxiliary medical means, implantable medical devices have attracted more and more academic attention. Based on the clinical application requirements for an implantable medical device, embedded space, energy supply, data communication and other key issues are discussed in this paper.

At present, two preoccupations of clinical application of implantable medical devices are as follows:

(i) The energy supply problem of the implanted unit in the body;

(ii) The data communication in vivo and vitro.

With the continuous development of wireless power transfer and wireless communication technology, power and data wireless transmission scheme has been the first choice for implantable medical devices. In the early days, most scholars used two groups of coils to transmit power and data, respectively. The communication quality is affected by the interference between the two sets of coils [1–6]. Wang et al. [4] and Zhou et al. [5] adopt orthogonal coils configuration to reduce the interference, whereas it is difficult to completely eliminate interference by using the orthogonal coils configuration. Another common problem is that the implanting space is limited. With the rapid development of integrated circuit technology, the contradiction between the volume of implanted antennas and limited space is great.

Received 7 March 2018, Accepted 28 April 2018, Scheduled 14 May 2018

* Corresponding author: Yuan Yang (762535409@qq.com).

The authors are with the Department of Electronic Engineering, Xi'an University of Technology, Xi'an, Shaanxi, China.

2. POWER AND DATA ARE TRANSMITTED WIRELESSLY WITH SAME CARRIER BASED ON HIGH-ORDER MODULATION

2.1. M-ary Differentially-Encoded Amplitude and Phase-Shift Keying (MDAPSK)

In view of the above two problems (interference and space), the scheme that single set of coils is used to realize power and data synchronously wireless transmission is proposed in this paper [7]. It is noteworthy that the power efficient transmission requires lower carrier frequency, while the data high-speed transmission needs higher carrier frequency. In order to resolve the frequency selective contradiction, the method of same carrier wireless transmission based on M-ary modulation is first proposed in this paper.

Firstly, the low carrier frequency is selected to realize the high efficient power transfer. Through M-ary modulation, the data transmission rate can be improved $\log_2^M$ times (M is modulating order), and the high speed data transmission is realized. Then, comprehensively considering the anti-noise capability and demodulation circuit complexity, MDAPSK modulation scheme is more suitable for the application environment of implantable medical devices [8, 9].

2.2. Experimental Verification of MDAPSK Modulation Scheme

In our experiment, the synchronous transmission of power and data is realized through a set of plane spiral coils. LED matrix is used to simulate the load of implantable medical devices. The error analyzer is used to test the quality of wireless communication. Fresh pork is used as biological channel, and the secondary coil is embedded in the pork to simulate the effect of implantation in vivo.

Based on field programmable gate array (FPGA) development platform (DE-4), functions including 16DAPSK modulation and demodulation, coding and decoding, A/D and D/A and error correcting are implemented. Class-E amplifier is designed and made. The D/A conversion signals amplified by the Class-E amplifier are loaded into the external primary coil for launch. Because the standard level of FPGA development platform is 3.3 V, and the standard level of error analyzer (AV5232E) is 5 V, special level transformation circuit is custom-made to ensure the level matching. The overall experimental system is shown in Figure 1.

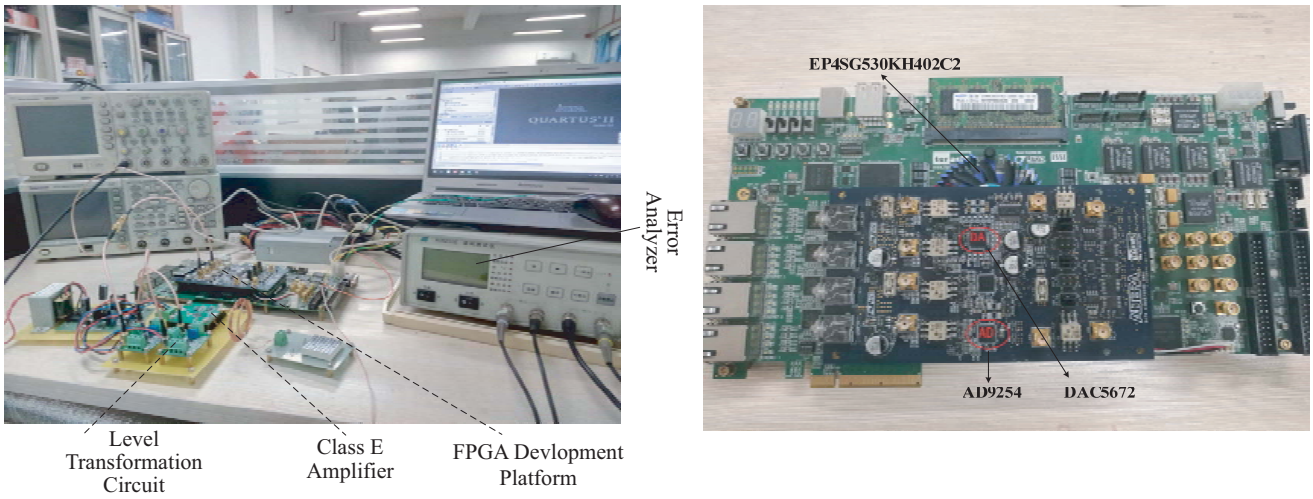

Figure 1. The complete picture of experimental circuit.

In order to verify the feasibility of the scheme, two experiments are carried out in air medium and biological medium, respectively. The experiment of power and data synchronous transmission in the air channel is shown in Figure 2.

The synchronous transmission carrier frequency is 16 MHz. Through Class-E amplifier, the power of primary coil transmitting signal is 1 W. The distance between primary coil and secondary coil is

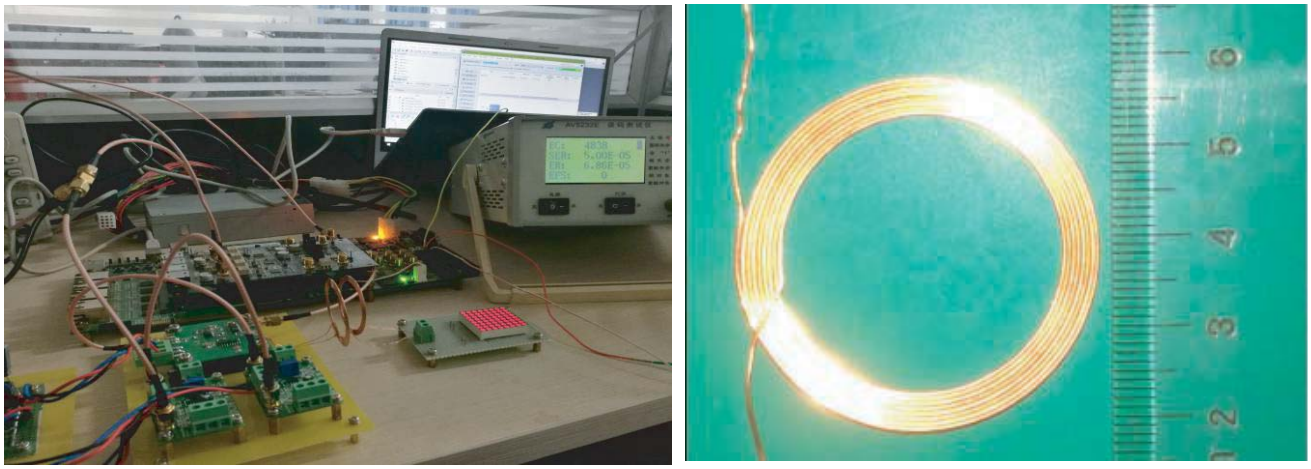

Figure 2. Power and data synchronous transmission in the air channel.

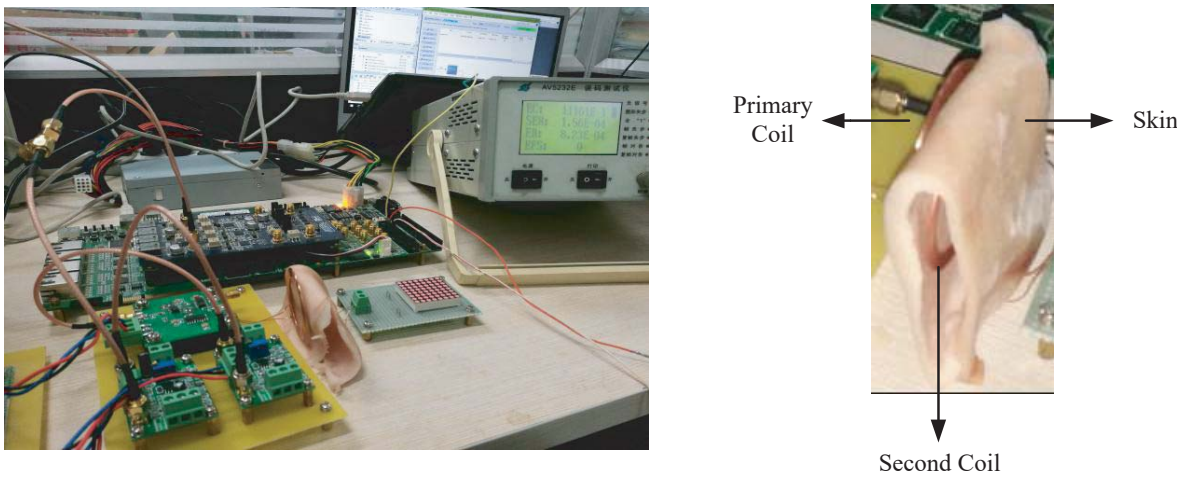

Figure 3. Power and data synchronous transmission in the skin channel.

1 cm. The received electromagnetic wave (EMW) is rectified, filtered and regulated. The obtained DC regulated power supply provides energy for the $8 * 8$ LED matrix. The experimental results show that the $8 * 8$ LED matrix is highly lit. Through analysis and computation, the power consumption of the matrix is 0.68 W. So, the power transfer efficiency is about 68% in air medium.

Next, wireless data transmission quality testing in air channel is carried out. The error analyzer generates random signals, and symbol rate is 2×10^6 Baud. Through 16MDAPSK modulation and D/A conversion, the signals are launched. The received analog signals are converted into digital signals, and then the signals are demodulated. The bit speed is 8 Mbit/s ($2M \times \log_2^{16} = 8$ Mbps). Error analyzer displays that bit error rate (BER) is 10^{-5}–10^{-6}.

In order to verify the feasibility of the proposed scheme in biological channel, secondary coil is embedded in fresh pig skin. Power and data transmission experiment is carried out again. The experimental results are shown in Figure 3.

Thickness of the pigskin between primary and secondary coils is 1 cm i.e., biological channel is 1 cm. Compared with Figure 2 and Figure 3, it is not hard to find that the LED matrix is still light, whereas the brightness is reduced. Through analysis and computation, the power consumption of the matrix was about 0.52 W. The power transmission efficiency in biological is reduced to 52%. At the same time, the BER display of the error analyzer is increased to 10^{-4}.

Compared with experimental results of air channel, the scheme is still valid in the biological tissue.

However, the transmission quality is worse. The reason lies in the influence of biological channel on energy and data wireless transmission. Therefore, when the secondary coil of implantable medical devices is implanted, the impact of biological tissue on the system deserves our attention.

3. CHARACTERISTICS RESEARCH AND MODEL OPTIMIZATION OF WIRELESS POWER TRANSFER IN BIOLOGICAL CHANNEL

3.1. Biological Channel Wireless Power Transfer System Modeling

Nikola Tesla first proposed the idea of wireless power transfer. Marin Soljačić then published an article in "Science". Strongly coupled magnetic resonance was used to realize the wireless power transfer [10]. Recently, the wireless power transfer technology has been applied to the practice [11, 12]. The simplest circuit topology is shown in Figure 4(a). V_s is the power source, Q_1 the quality factor of primary coil, Q_2 the quality factor of second coil, and i_1 and i_2 are primary loop current and second loop current, respectively.

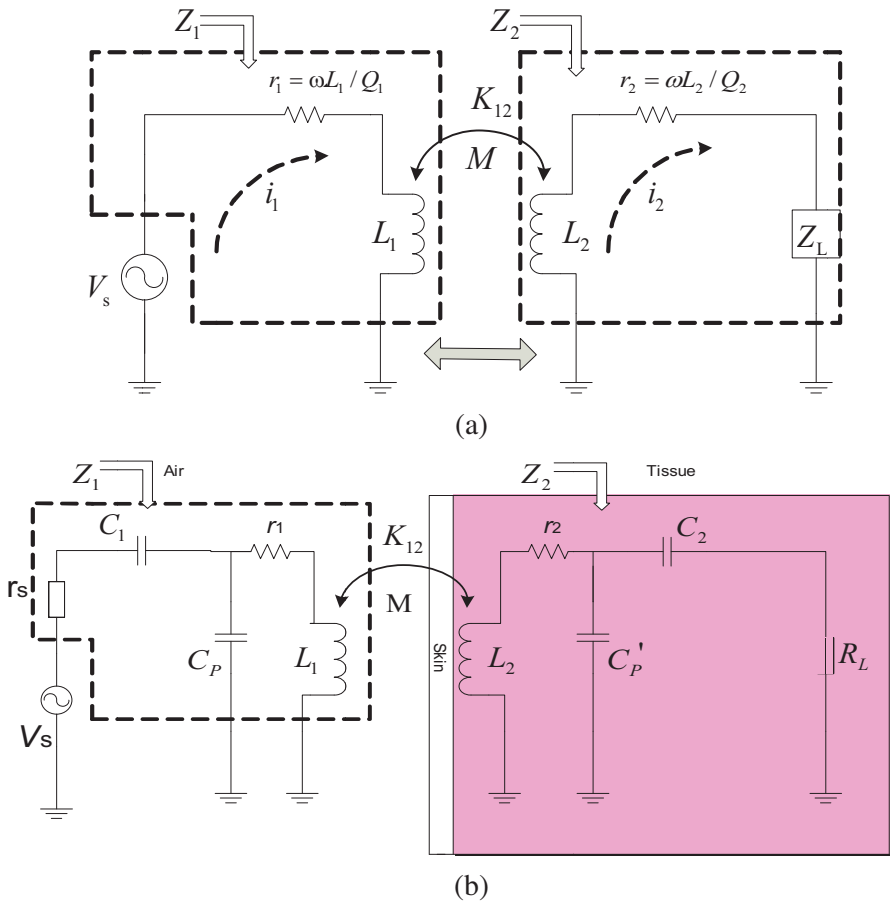

Figure 4. The system topology of WPT. (a) The simplest topology of inductance coupled wireless power transfer; (b) The topology of wireless power transfer system in biological channel.

The simplest mathematical model of wireless power transfer system is shown as Equation (1) [13].

$$\eta = \frac{\omega M^2 R_L / L_1}{\omega M^2 R_L / L_1 + \omega M^2 r_2 / L_1 + [(\omega L_2 + X_L)^2 + (r_2 + R_L)^2] r_1 / \omega L_1} \tag{1}$$

In the formula, η denotes power transfer efficiency; ω denotes the transfer angular frequency; M

means mutual inductance; L_1 and L_2 are the primary and secondary coil's inductance respectively; $R_L + j \cdot X_L = Z_L$ represents the load.

In order to realize energy supply for implantable medical devices, implanting a coil in the body is a widely used method. And the wireless power transfer is achieved through the coupling of internal and external coils. Considering the impact of biological tissue on wireless power transfer, the wireless power transfer topology of implantable medical device is shown in Figure 4(b).

In order to improve the wireless power transfer efficiency, compared with Figure (a), the matching capacitors C_1 and C_2 in Figure 4(b) are increased to realize resonant coupling transmission. In order to improve the accuracy of the model, the internal resistance of the power supply r_s and parasitic capacitor C_p is added. Moreover, bio-capacitor C'_p is first introduced to reflect the influence of biological tissue on the wireless power transfer.

The implanted coil is surrounded by biological tissue. The gap between two adjacent turns of coil is shown in Figure 5. D_c is the bare wire diameter, and D_o is the wire diameter with the insulating layer.

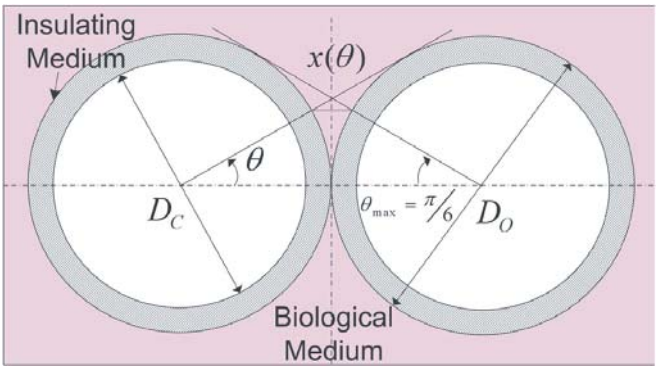

Figure 5. The cross section schematic between two adjacent turns of implanted secondary coil.

The bio-capacitance C'_p can be equivalent to a series of insulating layer equivalent capacitance C_{ttc} and biological layer equivalent capacitance C_{ttm}.

The insulating layer equivalent capacitance of per unit angle is expressed as [13]

$$dC_{ttc} = \frac{\varepsilon_r \varepsilon_0 l_t}{2 \ln \frac{D_o}{D_c}} d\theta \tag{2}$$

wherein, ε_0 is the air dielectric constant, ε_r the relative dielectric constant of coil covering and $\varepsilon_r \approx 3.5$, and l_t the corresponding effective length of two adjacent turns of the coil. The biological tissue equivalent capacitance of per unit angle is expressed as [13]

$$dC_{ttm} = \varepsilon_0 \varepsilon_m \frac{l_t D_o}{2x(\theta)} = \varepsilon_0 \varepsilon_m \frac{l_t}{2(1 - \cos\theta)} d\theta \tag{3}$$

where ε_m is the relative dielectric constant of biological tissues, $\varepsilon_m \gg 1$, and ε_m of different biological tissues at different frequency can be obtained by table lookup (http://niremf.ifac.cnr.it/tissprop/) [14].

The bio-capacitance of per unit angle thus can be derived as

$$dC'_p(\theta) = \frac{dC_{ttc} dC_{ttm}}{dC_{ttc} + dC_{ttm}} = \frac{\varepsilon_0 l_t}{2} \frac{1}{\frac{1}{\varepsilon_m} + \frac{1}{\varepsilon_r} \ln \frac{D_o}{D_c} - \frac{1}{\varepsilon_m} \cos\theta} d\theta \tag{4}$$

Therefore, the equivalent biological capacitance between two adjacent turns can be obtained by

integral operation.

$$C'_{tt} = 2\int_0^{\frac{\pi}{6}} dC'_{eq}(\theta) = \varepsilon_0 l_t \frac{2\varepsilon_r\varepsilon_m \arctan\left[\dfrac{\left(-1+\sqrt{3}\right)\varepsilon_m \ln\dfrac{D_o}{D_c}}{\left(1+\sqrt{3}\right)\sqrt{\left(2\varepsilon_r+\varepsilon_m \ln\dfrac{D_o}{D_c}\right)\varepsilon_m \ln\dfrac{D_o}{D_c}}}\right]}{\sqrt{\left(2\varepsilon_r+\varepsilon_m \ln\dfrac{D_o}{D_c}\right)\varepsilon_m \ln\dfrac{D_o}{D_c}}} \tag{5}$$

The bio-capacitance between the turns of the coil is connected in series, and the total bio-capacitance of the n-turn coil could be described as

$$C'_P = \frac{1}{\dfrac{1}{C'_{12}} + \dfrac{1}{C'_{23}} + \ldots + \dfrac{1}{C'_{n-1n}}} \tag{6}$$

Due to the influence of bio-capacitor, the theoretical matching capacitance of traditional resonant coupling scheme is shifted. Compared with the ideal expectation, the power transfer efficiency in biological medium is deviated seriously. The simulation contrast is shown in Figure 6.

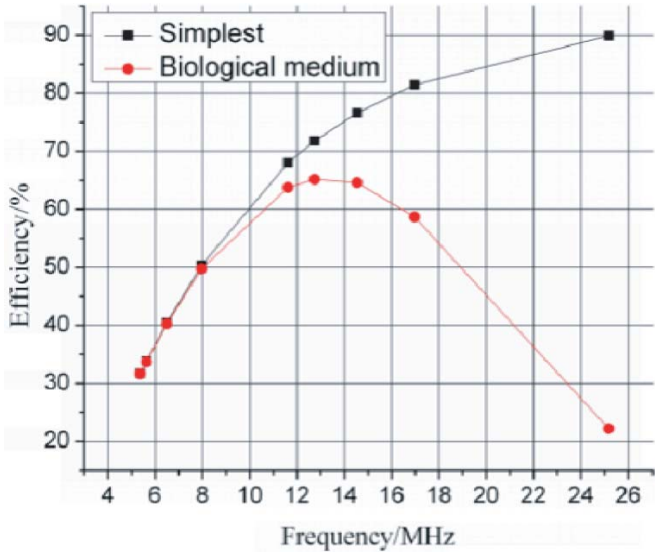

Figure 6. The comparison chart of power transfer efficiency simulation. The distance between the coils $D = 1\,\text{cm}$.

In order to verify the accuracy of the modeling, the experimental devices as shown in Figure 7 are used to measure the power transfer efficiency in biological channel.

Two frequency points, 16.97 MHz and 11.61 MHz, are selected randomly. With increasing the implantation depth of secondary coil (The thickness of biological tissue between the two coils is increased), the curve of power transfer efficiency is shown in Figure 8.

In the initial depth of the biological channel, the measured data and model data are highly consistent. With the increase of channel depth, the error between measured and model simulation increases. The reason is that the absorption energy of biological tissue is not considered in the above model.

3.2. Biological Path Attenuation Model

In this paper, Comsol Multiphysics is used to model and analyze the attenuation of electromagnetic energy in the biological path. Comsol Multiphysics is a multi-physical field comprehensive analysis

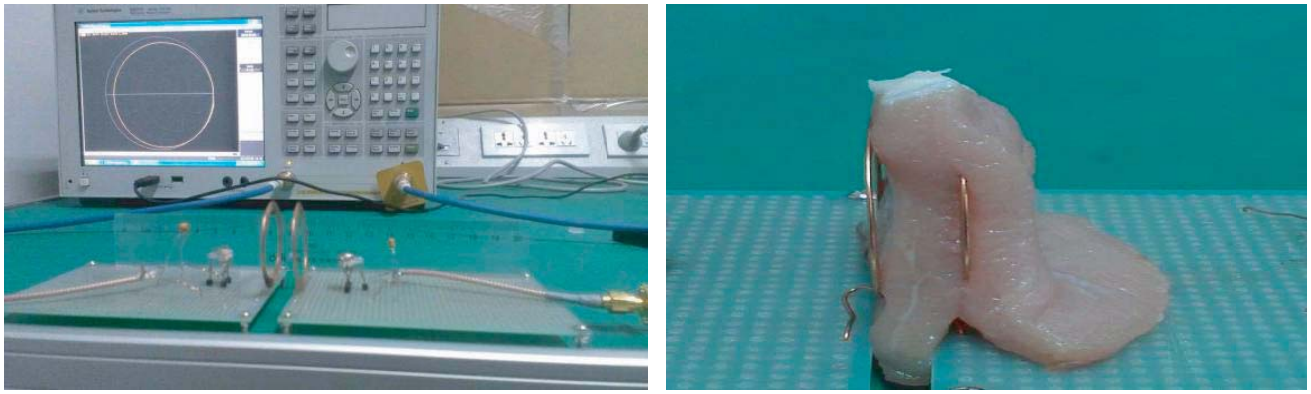

(a) (b)

Figure 7. The photos of experimental measurement device. (a) The general view of experiment devices; (b) The schematic of secondary coil is implanted.

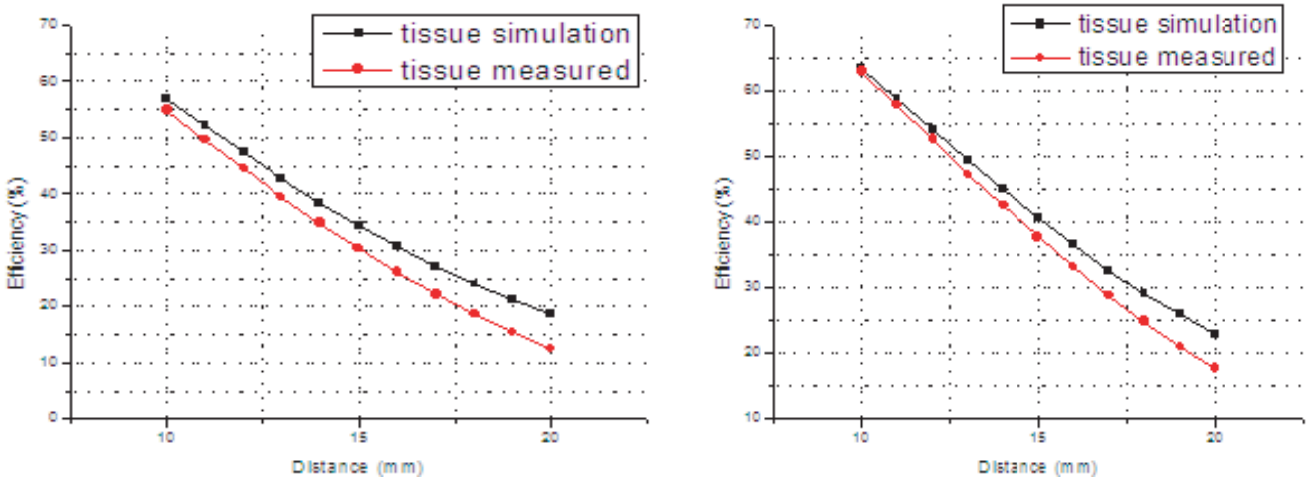

(a) (b)

Figure 8. The power transfer efficiency in biological medium. (a) The contrast of simulation and measured at 16.97 MHz; (b) The contrast of simulation and measured at 11.61 MHz.

software. First, using the software drawing tool, two 8-turn plane spiral coils are drawn to simulate internal and external coils, which are used to transmit and receive energy. The coils are ideal, and there are no skin and proximity effects. Then the multi-layer (single layer) cube is drawn to simulate heterogeneous (homogeneous) biological channel. In order to avoid the effect of electromagnetic wave reflection on the simulation results, the scattering boundary conditions (SBC) are selected. The model adopts adaptive mesh subdivision. The grid is divided into triangles, and the key area grid is further refined to enhance the precision of the model. The frequency dispersion characteristics of biological tissues are reflected by setting different frequency point conductivity and relative dielectric constant. The electromagnetic waves absorption characteristics of different biological tissues in different transmission frequencies are simulated. The model and simulation results are shown in Figure 9.

In order to meet the demand of power high-efficiency transfer and data high-speed transmission with same carrier, MHz frequency band is the only option [15–18]. The simulation data of 10–410 MHz spectrum are used to establish the biological path loss model in this paper. The spectrum contains several ISM (Industrial Scientific Medical) and MICS (Medical implant communication services) frequency points. Therefore, the model has wide range of engineering applications. The biological path loss model reflects the absorption effect of biological tissues on EMW. On one hand, it can improve the

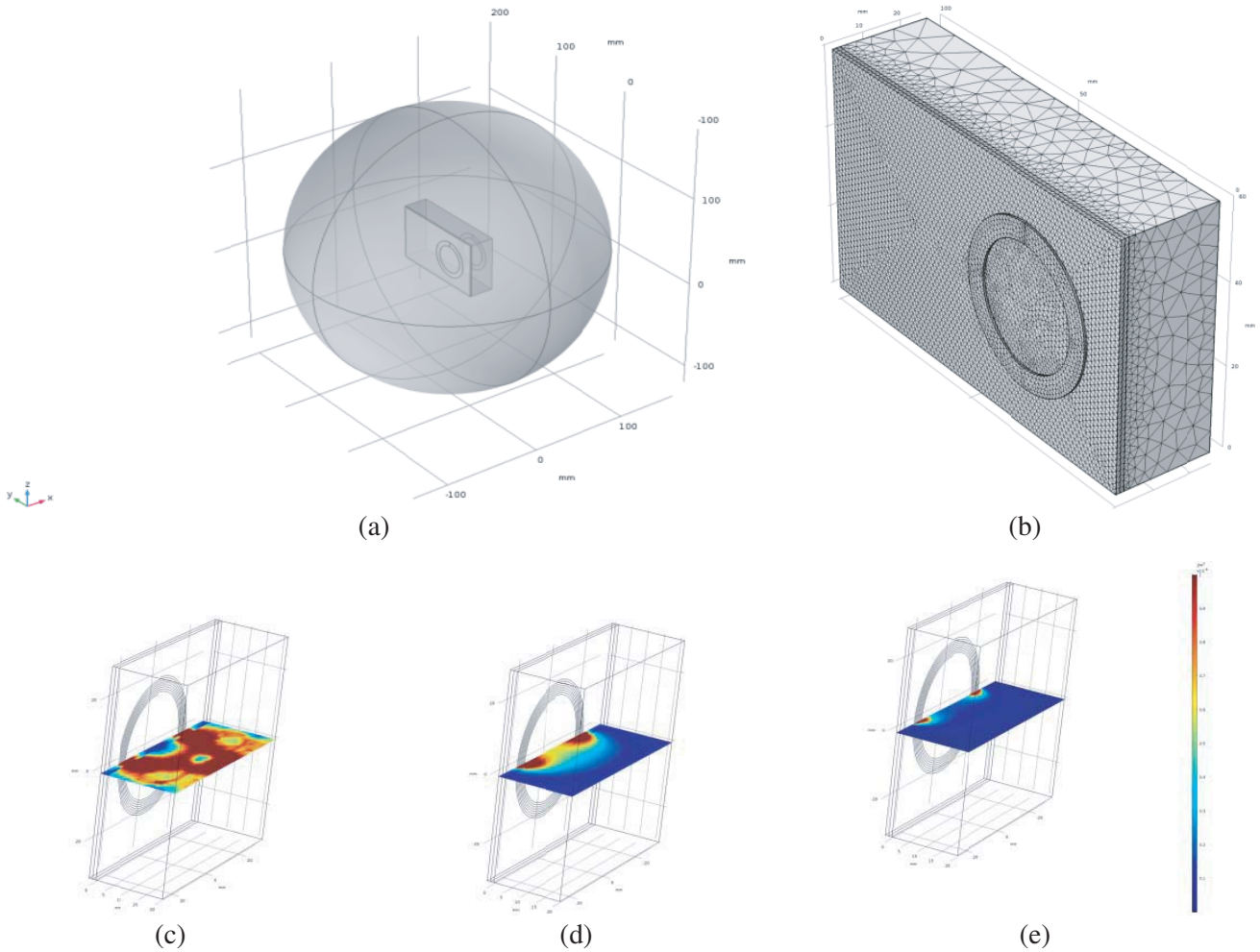

Figure 9. The diagram of model and simulation results based on COMSOL. (a) The full view of simulation model; (b) The mesh profile of coil and channel; (c) EMW attenuation trend at 13.56 MHz; (d) EMW attenuation trend at 402 MHz; (e) EMW attenuation trend at 2.457 GHz.

model accuracy of wireless power transfer system above. On the other hand, it is of great significance to the analysis of biological channel error rate below.

In this paper, COMSOL Multiphysics is adopted to obtain massive simulation data, using Levenberg-Marquardt algorithm, and the simulation data are fitted. The fitting results show that the attenuation trend of EMW in the homogeneous biological path can be approximately linear. The attenuation slope K is related to the biological tissue conductivity σ, relative dielectric constant ε and EMW incident energy density P (J/m^3). The homogeneous tissue path loss model is described as

$$K = P \times \left(\sum_{i=1}^{n} \left[p_i \sigma^i + q_i (\ln \varepsilon)^i \right] + m \right), \quad n = 1, 2, \ldots, 5 \tag{7}$$

wherein, p_i, q_i and m are constants: $p_1 = -0.0531$, $p_2 = -1.3092$, $p_3 = 4.8602$, $p_4 = -6.2840$, $p_5 = 2.7651$, $q_1 = -0.7012$, $q_2 = -0.4614$, $q_3 = 0.1434$, $q_4 = -0.0208$, $q_5 = 0.0011$, $m = -0.4076$.

The model of heterogeneous path loss is more complicated. At the junction of different biological tissues, there is a mutation in the slope of EMW attenuation. However, in the range of 10–410 MHz, the attenuation slope in each biological tissue is still approximately linear. The slope is indicated by the letter K', which is related to the slope before and after the mutation. K_f and K_b indicate the attenuation slope before and after the mutation, respectively. The heterogeneous biological tissue path

loss model is expressed as follows.

$$K' = \frac{a_1 + a_2 \cdot K_f + a_3 \cdot K_b}{1 + b_1 \cdot K_f + b_2 \cdot K_f^2 + b_3 \cdot K_b + b_4 \cdot K_b^2 + b_5 \cdot K_b^3} \tag{8}$$

wherein, a and b are constants: $a_1 = 0.0015$, $a_2 = 0.9179$, $a_3 = 1.4996$, b_1 =-92.6433, $b_2 = -3619.0503$, b_3 =-31.4373, $b_4 = -871.0130$, $b_5 = -7072.9235$.

In order to verify the reliability of the above mathematical models, we employ a 3-year-old male New Zealand white rabbit for the implanted experiments. The experimental environment is shown in Figure 10. The secondary coil is implanted into the different depths of right groin of the rabbit. A vector network analyzer (VNA, AV3619) is used to measure parameter S_{21}.

Figure 10. Demonstration of animal living experiment.

Experiment 1: the secondary coil is implanted into 8 mm depth of groin. The EMW propagation path is a heterogeneous path, which consists of 1 mm skin, 4 mm fat, and 3 mm muscle. When the wireless transfer frequency is selected as 50 MHz, the VNA shows that the energy receiving efficiency is -5.11 dB (30.83%).

Based on the above wireless power transfer model, due to the existence of the biological capacitance, the effect of traditional resonant coupling scheme is not ideal. The power transfer efficiency is only 37.95%. The error between the simulated and measured values is 7.12%. According to the biological path attenuation model, Equations (7) and (8), when 50 MHz EMW incident energy density is 1 J/m^3, the attenuation slope in skin is -0.0181. Through the 1 mm skin path, the remaining energy is 0.9819 J/m^3. Then, the EMW enters the fat layer, and the attenuation slope is -0.0097. Through the 4 mm fat path, the remaining energy is 0.9471 J/m^3. At last, the EMW enters the muscle layer, and the attenuation slope is -0.0174. Through the 3 mm muscle path, the terminal energy is 0.8949 J/m^3. Therefore, the biological path energy loss is 10.51%. With comprehensively considering the effects of biological capacitance and biological path attenuation, the simulation value of wireless power transfer efficiency is 27.44%. Compared with the measured value, the error is only 3.39%. After the model synthesis, the accuracy of the system is improved obviously.

Experiment 2: The skin and fat layers are peeled, and the muscle tissue is exposed. 13.56 MHz is selected as wireless transmission carrier frequency. Then the wireless power transfer efficiency in the muscle homogeneous channel is measured at 1, 2, 3, 5 and 7 mm. The measured values are -2.11 dB (61.47%), -3.39 dB (45.79%), -4.81 dB (33.06%), -7.68 dB (17.08%), -11.59 dB (6.93%). On this basis, the biological path loss model is superimposed. The linear attenuation slope in muscle tissue is $K = -0.0101$. The simulated and experimental values of energy transfer efficiency are shown in Figure 11. In the figure, x-axis is the channel depth (unit: mm), and y-axis is the power transfer efficiency.

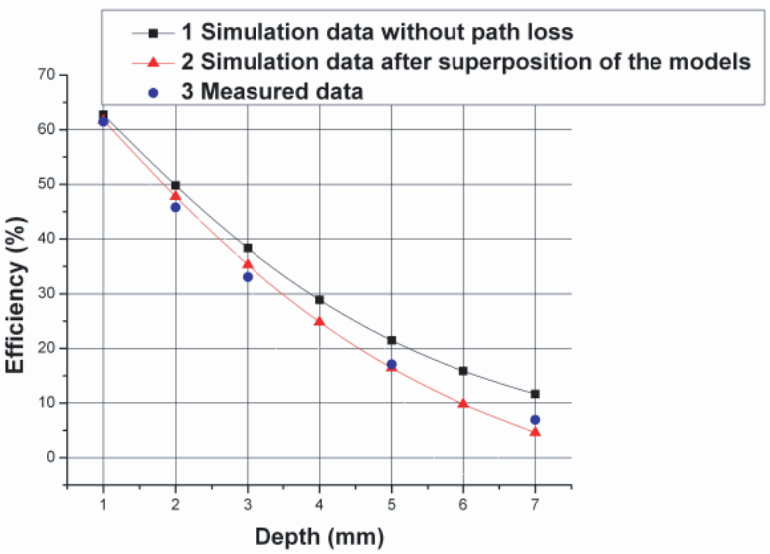

Figure 11. The comparison of the measurement and simulation of homogeneous biological path loss.

As can be seen from Figure 11, curve 1 is the simulation value that biological path loss is not considered. Curve 3 is the experimental measured values. It can be found that the error between simulated and measured values increases with the increase of biological path. However, curve 2 is obtained through the superimposed of wireless power transfer model and biological path loss model. The error between simulation and measurement is significantly reduced.

4. THE WIRELESS DATA COMMUNICATION OUTLOOK OF BIOLOGICAL CHANNEL

The path loss of biological medium has influence on channel attenuation factor. Moreover, the path loss affects system signal-to-noise ratio (SNR). Therefore, the modeling of path loss lays the foundation for the analysis of the error rate of biological channel.

In order to reduce error rate and improve communication quality, two aspects of work can be carried out:

(i) In order to ensure high SNR, time division multiplexing can be adopted to realize the data and power wireless transfer without overlapping in time domain.

(ii) Soft demodulation and RS$(15, 9)$ soft decoding schemes can be employed to suppress and correct errors.

5. CONCLUSION

A high-order differential modulation (16DAPSK) scheme is used in this paper to balance the selection frequency contradiction between the energy high-efficient transfer and data high-speed transmission. The scheme makes it possible that implantable medical devices wirelessly transmit power and data simultaneously with one group of coils. In the aspect of power and data transmission system modeling, this paper introduces biological capacitor model, which can accurately reflect the influence of matched capacitance migration on resonant coupling transmission efficiency. Then the model precision of the wireless power transfer system is further improved by the superposition of the biological path loss model. Based on the biological path loss model and the error generation mechanism of 16DAPSK, we can establish an accurate biological channel error rate analysis model in future work.

In this paper, the power and data simultaneous wireless transmission scheme based on MDAPSK is proposed. The analysis models about power transmission and biological path loss are established. This paper provides a new solution and models reference for implantable medical devices clinical application.

ACKNOWLEDGMENT

This work was supported in part by the National Natural Science Foundation of China (No. 61102017) and Doctorial Innovation Fund of Xi'an University of Technology (No. 310-11202j406), Natural science special project of Shaanxi Province Education Department (No. 16JK1576), The Industrial Public Relation Project of Shaanxi (No. 2017GY-083).

REFERENCES

1. Jung, L. H., P. Byrnes-Preston, R. Hessler, T. Lehmann, G. J. Suaning, and N. H. Lovell, "A dual band wireless power and FSK data telemetry for biomedical implants," *Proceedings of the IEEE International Conference on Engineering in Medicine & Biology Society Lyon*, 6596–6599, France, August 23–26, 2007.
2. Ghenim, A., D. Daoud, M. Ghorbel, A. B. Hamida, and J. Tomas, "A dual band wireless power and DPSK data telemetry for biomedical implants," *Proceedings of the International Conference on Microelectronics*, 1–5, Tunisia, December 19–22, 2011.
3. Ramrakhyani, A. K. and G. Lazzi, *Wireless Applications: Dual Band Power and Data Telemetry*, Springer, New York, 2015.
4. Wang, G., P. Wang, Y. Tang, and W. Liu, "Analysis of dual band power and data telemetry for biomedical implants," *IEEE Transactions on Biomedical Circuits & Systems*, Vol. 6, 208–215, 2012.
5. Zhou, M., M. R. Yuce, and W. Liu, "A non-coherent dpsk data receiver with interference cancellation for dual-band transcutaneous telemetries," *IEEE Journal of Solid-State Circuits*, Vol. 43, 2003–2012, 2008.
6. Wang, G., W. Liu, M. Sivaprakasam, M. Zhou, J. D. Weiland, and M. S. Humayun, "A dual band wireless power and data telemetry for retinal prosthesis," *Proceedings of the IEEE International Conference on Engineering in Medicine and Biology Society*, 4392–4395, New York, USA, August 30–September 3, 2006.
7. Li, X., Y. Yang, N. Yu, and S. Qiao, "Simultaneous energy and data wireless transfer attenuation in biological channel of deep implantable medical devices: Characteristic analysis and modeling," *Progress In Electromagnetics Research M*, Vol. 56, 169–177, 2017.
8. Qin, Y. J., H. Kiyoshi, and Y. A. Liu, "A novel demodulation decoding method for coded 16dapsk signals," *Journal of Electronics & Information Technology*, Vol. 28, 1645–1648, 2006.
9. Adachi, F., "Error rate analysis of differentially encoded and detected 16apsk under rician fading," *IEEE Transactions on Vehicular Technology*, Vol. 45, 1–11, 2002.
10. Kurs, A., A. Karalis, R. Moffatt, J. D. Joannopoulos, P. Fisher, and M. Soljacic, "Wireless power transfer via strongly coupled magnetic resonances," *Science*, Vol. 317, 83–86, 2007.
11. Zlatanov, N., D. W. K. Ng, and R. Schober, "Capacity of the two-hop relay channel with wireless energy transfer from relay to source and energy transmission cost," *IEEE Transactions on Wireless Communications*, Vol. 16, 647–662, 2016.
12. Maehara, D., G. K. Tran, K. Sakaguchi, and K. Araki, "Experimental study on battery-less sensor network activated by multi-point wireless energy transmission," *IEICE Transactions on Communications*, Vol. E99.B, No. 4, 135–150, 2016.
13. Li, X., Y. Yang, and Y. Gao, "Visual prosthesis wireless energy transfer system optimal modeling," *Biomedical Engineering Online*, Vol. 13, 1–11, 2014.
14. Gabriel, S., R. W. Lau, and C. Gabriel, "The dielectric properties of biological tissues: III. Parametric models for the dielectric spectrum of tissues. *Physics in Medicine & Biology*, Vol. 41, 2271–2293, 1996.
15. Chen, K., Z. Yang, L. Hoang, J. Weiland, M. Humayun, and W. Liu, "An integrated 256-channel epiretinal prosthesis," *IEEE Journal of Solid-State Circuits*, Vol. 45, 1946–1956, 2010.
16. Khaleghi, A., R. Chavez-Santiago, and I. Balasingham, "Ultra-wideband pulse-based data communications for medical implants," *IET Communications*, Vol. 4, 1889–1897, 2010.

17. Chae, M. S., Z. Yang, M. R. Yuce, L. Hoang, and W. Liu, "A 128-channel 6 mw wireless neural recording ic with spike feature extraction and uwb transmitter," *IEEE Transactions on Neural Systems & Rehabilitation Engineering*, Vol. 17, 312–321, 2009.
18. Li, X., C. Y. Tsui, and W. H. Ki, "A 13.56 MHz wireless power transfer system with reconfigurable resonant regulating rectifier and wireless power control for implantable medical devices," *IEEE Journal of Solid-State Circuits*, Vol. 50, 978–989, 2015.